BILINGUAL PUBLISHING CO.
Pioneer of Global Academics Since 1984

Journal of Mechanical Engineering Research
https://ojs.bilpublishing.com/index.php/jmer

ARTICLE

Analysis of Autogenous Laser Welding in Low Carbon and Large Thickness Steel

Daniel Kohls[1] Carlos Enrique Ninõ Bohorquez[2] Enori Gemilli[3] Majorie Anacleto Bernardo[4*]

1. Federal University of Santa Catarina, Block A of the Department, Florianopolis, SC, 88.040-900, Brazil
2. Department of Mechanical Engineering, State University of Santa Catarina, Rua Paulo Malschitzki, Zona Industrial, Joinville, SC, 89.219-710, Brazil
3. State University of Santa Catarina, Rua Paulo Malschitzki, Zona Industrial, Joinville, SC, 89.219-710, Brazil
4. Federal University of Santa Catarina, Centro Block A of the Department, Florianopolis, SC, 88.040-900, Brazil

ARTICLE INFO

Article history
Received: 21 June 2021
Accepted: 27 July 2021
Published Online: 25 August 2021

Keywords:
Autogenous LASER welding
Welding of thick joints
Keyhole stability

ABSTRACT

With the use of laser welding, it is possible to join different steel, with different thicknesses, with or without the action of protective layers. The quality of laser radiation makes it possible to get certain characteristics that are impossible to get by other processes, such as high welding speeds, less metallurgical effects suffered by the heat-affected zone (ZAC), and this process also does not require filler metal, therefore it is free from possible contamination.

Combined with traditional welding methods, laser welding produces narrower weld beads, allowing for better prevention of corrosion and thermal distortions.

Although the process already has high industrial knowledge, some random defects, such as porosities and inconsistencies, are still found. This work presents a systematic study to determine the influence of laser welding parameters and how these parameters influence welding defects. For this, the experimental part was carried out in the welding laboratory - LABSOLDA, of the Federal University of Santa Catarina - UFSC, during the laser welding processes, a welding speed of 2.4 m/min was reached. For this experiment, argon was used as a shielding gas and 1020 steel was used as the base material.

1. Introduction

Welding is the most used process of joining metallic materials in the world, because of its vast practicality and ease, almost all production principles use welding in their production processes. Besides the production processes, welding is heavily used in equipment maintenance and recovery. One of the great advantages of welding is to get the union of materials, maintaining not only the external appearance but also the continuity of chemical and mechanical properties.

Theoretical Foundation

In 1960, Theodore Maiman [1] presented the first Laser light emission (Light Amplification by Stimulated

**Corresponding Author:*
Majorie Anacleto Bernardo,
Federal University of Santa Catarina, Centro Block A of the Department, Florianopolis, SC, 88.040-900, Brazil;
Email: anacletomajorie@gmail.com

 DOI: https://doi.org/10.30564/jmer.v4i2.3381

Emission of Radiation). This was the first emission located in the visible range of the electromagnetic spectrum. Since then, the development of this technique for application in the industry has been continuous and encouraged by the good results achieved.

Since then, the development of the potential for application in the industry has been continuous and encouraged by the results achieved.

The physical principle of laser light, or stimulated emission of light came from the theory planned by AlbertEinstein, which postulated that the quantization of energy from harmonic oscillators could also be given as if light comprised "quanta" of energy, and light passed to be described as made up by small amounts of electromagnetic energy, or by photons with the same wavelength, synchronous, and in the same direction and direction as an incident photon as a form of stimulus [2].

The laser welding process involves focusing a high-power beam on a small area, which can generate intensities greater than 104 W/mm^2. At these power levels, the material vaporizes at the laser's focal point creating a cavity called a keyhole. This cavity helps to transmit the beam into the material by multiple reflections, which increases the coupling between the beam and the material (increased absorptivity) [3].

This stimulated emission should, however, have higher rates than the spontaneous absorption and emission to ensure a larger possible amount of atoms in the excited state to produce another identical photon (light) with the same energy and in phase, in the direction of the incident photon that constitutes the laser beam.

Phenomena such as light reflection and absorption, heat conduction, enable better adequacy of the production process and the choice of material to be worked, influence the laser process, which is related to optical and thermal properties, and not to the mechanical proprieties [4].

Reflectivity, which is the index indicative of the portion of the incident light beam reflected by the workpiece material, can vary with the wavelength of laser radiation. Materials such as aluminum and copper have high reflectivity, which makes laser processing and application difficult. However, as the surface temperature increases, the reflectivity decreases, which forms a reflectivity-minimizing feature.

Figure 1 shows the laser welding process. This stimulated emission should, however, have higher rates than the spontaneous absorption and emission to ensure a larger possible amount of atoms in the excited state to produce another identical photon (light) with the same energy and in phase, in the direction of the incident photon that constitutes the laser beam.

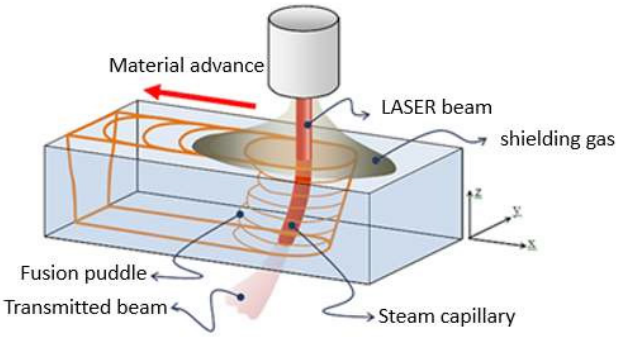

Figure 1. Illustration of the laser welding process

Source: Adapted from MIRIM, 2011

As the laser beam moves to create the bead, materials continuously fused in front of the beam, flowing around the keyhole and solidifying at the back of the weld pool. The intrinsic characteristics of penetration welding establish the maximum and minimum for the process speed: top speeds cause the keyhole to collapse, while very low speeds cause burrs and holes due to the liquid flow [5].

An important concept in welding is welding energy (E) which is defined as the heat given to the weld joint per unit of length (J/mm). The higher the welding energy, the larger the grain size of the molten zone and the larger the heat-affected zone (ZAC). For slower cooling speeds, grains in the region close to the melting line grows. In processes where low values of welding energy are involved, such as in Laser welding, the heat-affected zone (ZAC) is narrow and rarely has a defined grain growth region [6].

In laser welding, there are basically two different techniques, namely conduction welding and penetration welding or Keyhole. The energy density characterizes conduction welding being below 106 W/cm², not generating significant evaporation of the material, only a change in state from solid to liquid [7].

In the penetration welding process, higher energy densities than conduction welding characterize it (between 106 W/cm² and 109 W/cm²), and it is possible to carry out welding of components with great thickness. The difference between the welding techniques can be seen in Figure 2.

For welding low carbon steels, they're characterized by low strength and hardness, high tenacity, and ductility. They have good machinability, good weldability and are not heat-treated, besides requiring attention in the generation of discontinuities due to the absence (or low percentage) of alloying elements, such as Mn. Besides the low metallurgical complexity, low carbon steels have a simple chemical composition where they do not cause major microstructural changes in the heat-affected zone

DOI: https://doi.org/10.30564/jmer.v4i2.3381

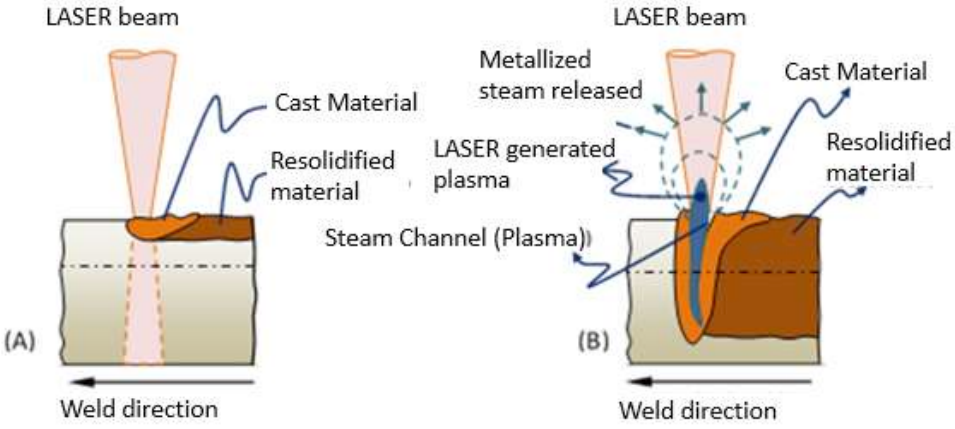

Figure 2. Representation of the conduction welding process (A) and penetration welding (B)

Source: Adapted from ENGEMANN, 1993.

(ZAC). The fusion and solidification of the material does not cause transformations in the crystalline structure that harm the characteristics of the welded joint, having a part without defects and properties and performance required for application [8].

2. Purpose

The objective of this work is to qualify the applicability of the 10 kW IPG fiber laser model YLS-10000 as a processing tool in the autogenous laser welding of thick and low-carbon structural steel joints, varying the laser input parameters and evaluating the metallurgical properties of the welded joints got.

Measure the output variables of the process by analyzing the heat-affected zone (ZAC) and the molten zone of the processed material after interaction with the laser beam between the power of 10 kW at the speed of 2.4 m/min and focus -6 mm. These theoretical-experimental analyses based on empirical information from [9], carried out in the same laboratory, as well as previous experimental procedures.

3. Methodology

The experimental ordering consists of carrying out controlled tests based on the survey and admissible parameters, which result in a good weld quality (without cracks and porosity) and with total penetration into the welded joint. The controlled tests were carried out from the interaction of the Laser light beam with a solid plate just forming a bead on a plate. An important point to be investigated in this work is keyhole stabilization.

The present work was carried out using a10 kW IPG fiber Laser system as a tool for laser welding. The methods comprise carrying out controlled tests, to make a list of admissible parameters, to have weld quality, without cracks and porosity, and with total penetration.

As a base material for welding, SAE 1020 steel was used, which is widely used in the industry in general, whether automotive, civil, naval, or machinery, and as an advantage it has a low cost compared to other steels and alloys because it is a steel with low content of carbon, meeting the requirements proposed in this work.

In Table 1 the chemical composition of SAE 1020 steel presented, according to the Brazilian standard that establishes the numerical designation used to identify carbon and alloy steels, according to their chemical composition (ABNT NBR NM 87: 2000) [10], data on the percentage of chemical elements present in 1020 steel was showed by the manufacturer Gerdal (supplier).

Table 1. Composition of SAE 1020 steel

Element	C (Carbon)	Mn (Manganese)	P (Phosphor)	S (Sulfur)
% (Standard)	0,18 - 0,23	0,30 - 0,60	≤ 0,030	≤0,050
% (Provider)	0,18 - 0,23	0,30 - 0,60	≤ 0,040	≤0,050

Source: SOUZA, 2017.

The 1020 steel plate used in this work has dimensions of 400 x 127 mm with a thickness of 3/8" (value with an order of magnitude suitable for drawing conclusions about the behavior of autogenous high-depth laser welding (thick joint) from a fiber laser source with 10 kW power).

In Figure 3, the distribution of the specimens on the 3/8" plates is observed so that, after welding, these specimens were removed by cutting with a water jet. Specimens in the plate's layout, the samples destined for

 DOI: https://doi.org/10.30564/jmer.v4i2.3381

Charpy tests in the regions of the welded joints, as well as the samples used for tensile testing in the same region and finally the samples used for tensile testing of the base material are notorious. For hardness and metallography tests, the same specimens mentioned above will be used.

3.1 Reviews

Evaluating and measuring the output parameters carried the verification of the quality of penetration of the laser beam into the welded parts out, carried out through visual inspection, with the naked eye and the analysis of micrographs (optical microscopy). To verify the microstructure, metallographic preparation of parts of the specimens is necessary.

The samples were prepared on the premises of the Metallographic Preparation Laboratory.Sample preparation was carried out following conventional metallography procedures, following the technical standards showed. In the sanding, the particle sizes 80,120,220,400, 600,800, 1200 were used in sequence. The samples were polished with 1 µm Alumina until reaching the desired surface quality. To allow the visualization of the microstructure of the material, a chemical attack was carried out with Nital 2% reagent (2% HNO_3 by volume of ethanol) for 15 seconds on the surface to be analyzed [11].

The quality verification of laser beam penetration into welded parts was carried out by evaluating and measuring the output parameters, carried out through visual inspection and the analysis of destructive and non-destructive tests discussed in the subsequent items.

3.1.1 Destructive Tests

Charpy traction and impact tests (type A) were performed at room temperature. The purpose of the first test is to evaluate the mechanical strength and ductility of the solder joint and the base metal. Normally, for thin joints, the specimen is removed transversally to the weld bead. For each of the situations, the analysis of the resistance to the last and the stretching was performed to determine the possibility of use or not.

For tensile tests performed in accordance with the Brazilian standard for carrying out tensile tests - ASTM A370-10 [12]. They were performed on an Instron 300LX-C4-J3D instrument. For base metal, a specimen was extracted from the rolled profile in the longitudinal direction of the rolling direction. The respective dimension for this test piece with rectangular cross-section is specified in Figure 4.

Regarding the tensile tests for welded joints, three specimens were extracted for each weld specification in the transverse direction to the lamination of the base metal. The respective dimensions can be seen in Figure 5.

For approval under the API 1104 [13] standard, which standardizes gas and arc welding processes for low-alloy steels, welded joints must meet the following criteria for rupture outside the welded joint and in the welded joint:

a) Breakage outside the welded joint: the breaking limit must meet the minimum strength limit of the base material specification;

b) Breakage in the welded joint: the rupture limit must meet the minimum strength limit of the pipe material specification, as well as in the fracture cross section: no pores larger than 1.6 mm (with the sum of the area not exceeding 2% of the fracture area) and the slag inclusions should not be more than 0.8 mm thick or more than 3 mm long, with a minimum separation of 13 mm between adjacent inclusions.

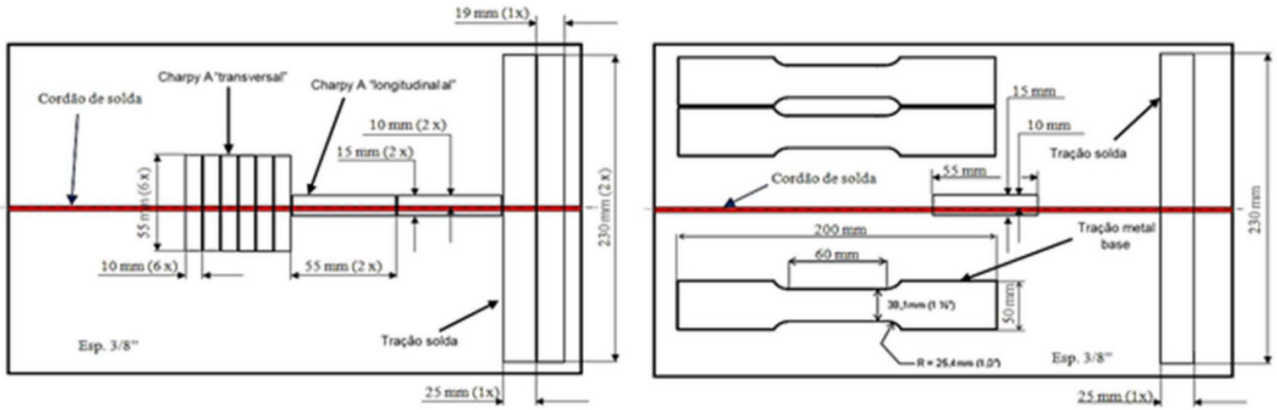

Figure 3. 3/8" x 400 x 127 mm plates intended for autogenous welding, which will be extracted by water cutting the specimens for Charpy A testing and traction on the base metal and welded joint

Source: Prepared by the authors, 2021.

DOI: https://doi.org/10.30564/jmer.v4i2.3381

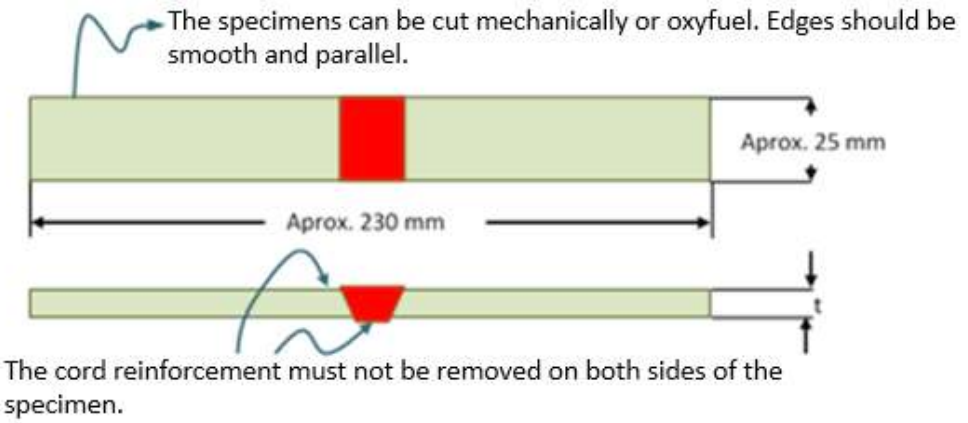

Figure 4. Dimensions of the tensile test specimens for the base metal, with thickness t = 9.54 mm (adapted from API 5L standard, 2007).

Source: Prepared by the authors, 2021.

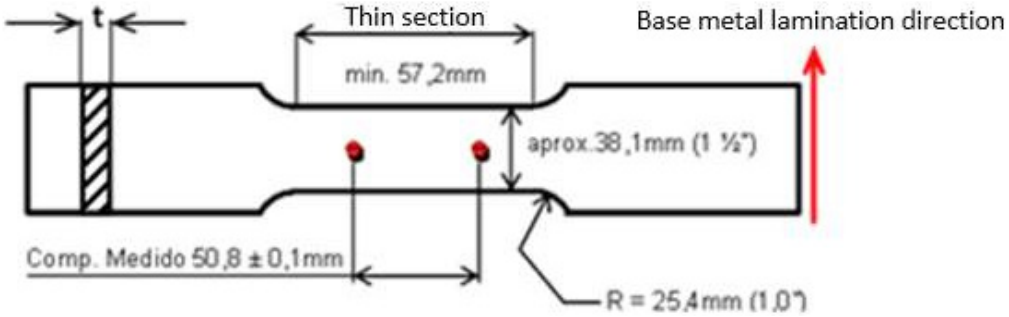

Figure 5. Representation of the tensile test body for the welded joints with the respective characteristic dimensions, being the thickness t = 9.54 mm.

Source: Prepared by the authors, 2021.

For the Charpy type A test, with a V-notch, it was made on the base metal, and in the welded region with the notches in the molten zone and in the heat-affected zone (ZAC), at room temperature as a variation of the ASTM E370 [14] standard in the dimensions of 10 mm x 10 mm x 55 mm, with three replicas for each condition analyzed. The notch was positioned in the thickness plane at positions relative to the center of the weld bead, heat-affected zone (ZAC).

The tests were carried out on the Wolpert universal impact testing machine; with three specimens for each welded joint in the longitudinal direction of the weld bead in the heat-affected zone (ZAC) and molten zone regions and in the transverse direction of the joint. The dimensions of the specimens and the representation of the welded profiles can be seen in Figure 6.

3.1.2 Non-destructive Testing

For the analysis of the macro and microstructure, the metallographic test was carried out by preparing sections of the specimens containing the welded regions of interest according to conventional procedures according to the technical standards indicated.

In the experimental procedure, sanding sectioned transversally and prepared the welded joints following the particle sizes 80, 120, 220, 400, 600, 800, 1200 respectively, with the samples being polished with 1 µm alumina until reaching the desired surface quality. The chemical attack was carried out with Nital 2% (2% HNO3 by volume of ethanol) for 15 seconds on the surface to be analyzed [11].

Vickers hardness tests (HV) were performed using a Future-Tech microhardness tester, model FM-800, and following the guidance of the ASTM E92-82 [15] standard. They were tested for each region of interest, base metal, heat-affected zone, and steel melt zone in the plane normal to the rolling direction and to the weld bead, as seen in Figure 7. In the procedure to get the hardness, a load of 500 g was used for a time of 15 seconds and a distance between impressions of 0.15 mm.

 DOI: https://doi.org/10.30564/jmer.v4i2.3381

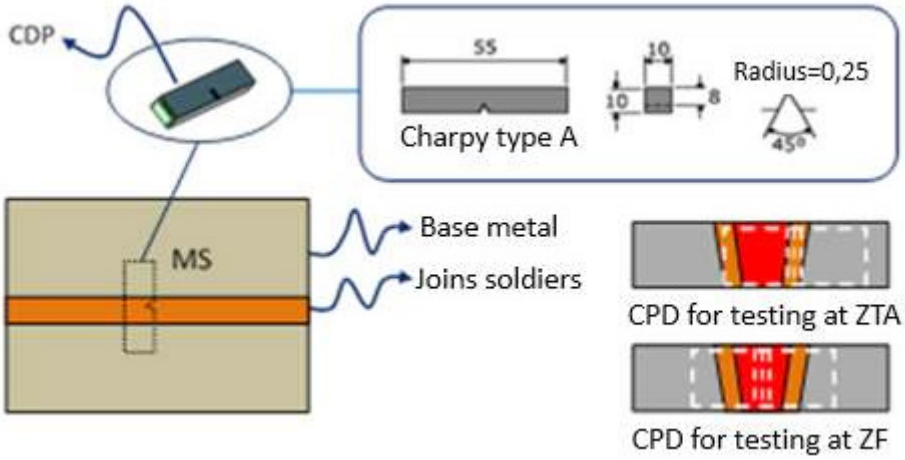

Figure 6. Representation of the specimen for the Charpy type A impact test with their respective dimensions taken from the welded material in the laser process and from the joins soldiers.

Source: Prepared by the authors, 2021.

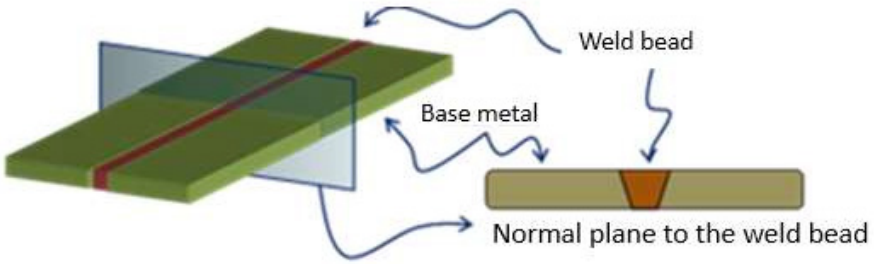

Figure 7. Representation of the planes for obtaining the Vikers hardness in the welded specimen

Source: Prepared by the authors, 2021.

4. Results

This chapter describes the experimental results obtained from the techniques seen in item 3 for destructive (tensile and Charpy A) and non-destructive (metallographic, hardness and Vickers microhardness) tests.

5. Discussion

5.1 Metallographic Test

For the macrograph verification of the welds, (Figure 8), it is verified that the width of the zone is affected by the heat-affected zone (ZAC) varies a lot: it is smaller in the root region and larger in the intermediate region (half the thickness). It is plausible that this is associated with differences in cooling rates across thickness and, as a result, differences in microstructure and hardness.

In Figure 9, there is a micrograph of the welded joint at a magnification of 50 x, where the appearance of the weld in the regions of the base metal, heat-affected zone(ZAC) and molten zone is observed. Visual inspection of the section shows the presence of porosity.

In the micrograph of Figure 10, the ferrite-pearlite microstructure, characteristic of 1020 steel, can be seen. The molten zone is also more clearly observed, indicated by point (A) and characterized by the presence of larger grains, heat-affected zone (ZAC), indicated by (B) and the base metal, region indicated by point (C), not affected by the high temperature in the welding process.

5.2 Hardness Test

Due to the variation in the width of the welding profile verified in Figure 8, three hardness profiles were made, parallel to the plate surface and at different depths. As the penetration of the welds was around 7 mm, the profiles were made at the following distances measured from the surface of the sheet: 1 mm; 3.5mm and 6mm.

The hardness profiles included 3 measurement points in the molten zone and the other 6 or 7 remaining in the heat-affected zone (ZAC), and base metal, as shown in Figure 11. The values are presented in Table 2, in which the zones in which the hardness are located base metal, heat-affected zone, and steel melt zone are identified.

DOI: https://doi.org/10.30564/jmer.v4i2.3381

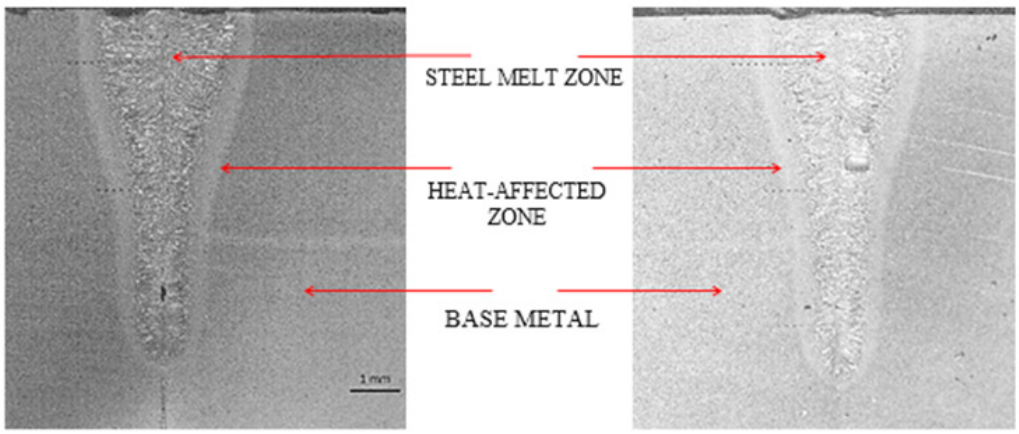

Figure 8. Macrographs of the cross sections of the welds performed with: a) low energy; b) high energy.

Source: Prepared by the authors, 2021.

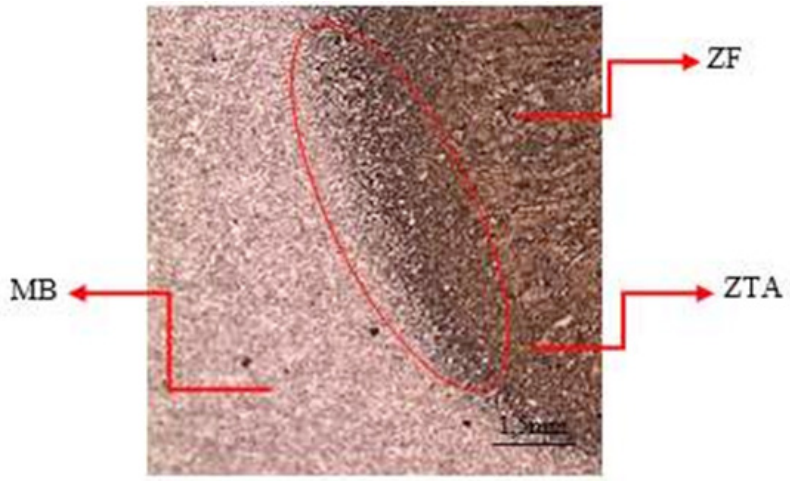

Figure 9. Micrograph of the welded joint at 50x magnification

Source: Prepared by the authors, 2021.

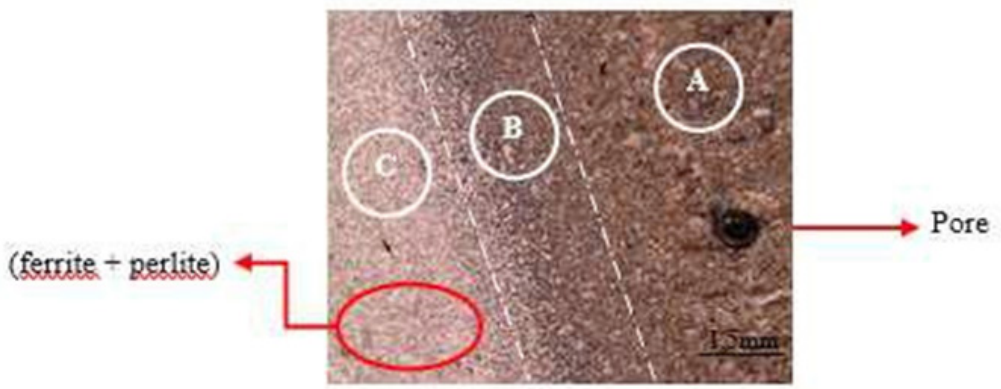

Figure 10. Micrograph of the welded joint at 50x magnification

Source: Prepared by the authors, 2021.

 DOI: https://doi.org/10.30564/jmer.v4i2.3381

Table 2. Values of microhardness of the welded joint profile in which the hardness zones located base metal, heat-affected zone, and steel melt zone are identified.

Region	Average Hardness (HV) Face profile	Region	Average Hardness (HV) Intermediate profile	Region	Average Hardness (HV) Root profile
Base metal	161	Base metal	180	Base metal	195
Heat-affected zone	234,6	Heat-affected zone	238,8	Heat-affected zone	314
Steel melting zone	324,2	Steel melting zone	332,7	Steel melting zone	405,7

Source: Prepared by the authors, 2021.

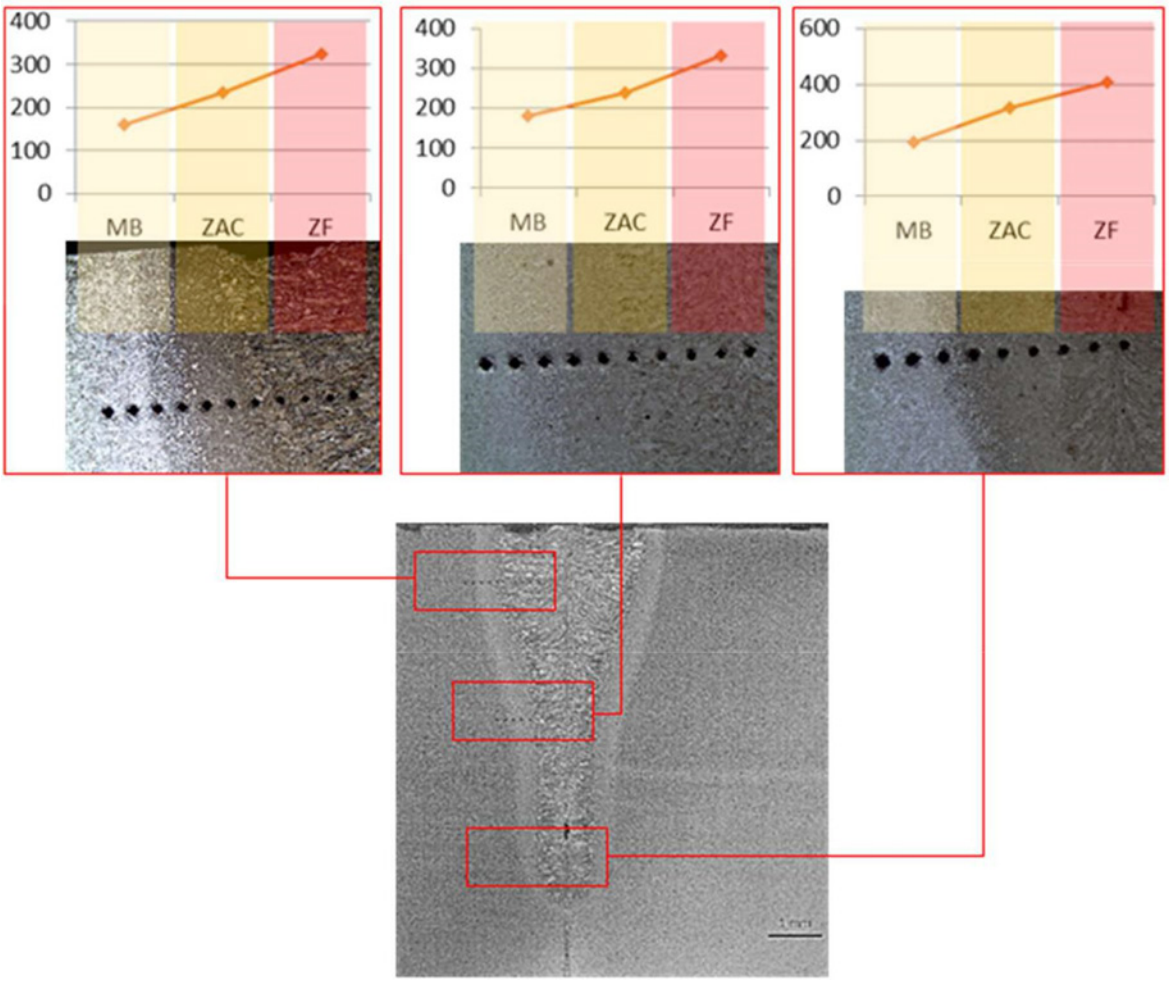

Figure 11. Representation of the hardness profiles carried out, with the identification points to determine the Vikers microhardness profile with the average of three points at three levels for the base metal, Thermally Affected Zone (ZTA) and molten zone.

Source: Prepared by the authors, 2021.

Regarding the verification of a relatively lower hardness of MB, the result was already expected because it is 1020 steel, but in heat-affected zone (ZAC), there was a high increase, due to the possible formation of martensite. In other words, even though the material has low hardenability, the high cooling rates resulting from the use of the laser promoted the formation of martensite.

5.3 Charpy Impact Test

The major result of the Charpy test is the energy needed to deform and fracture the specimen, called the global energy, which is read directly on the machine's

DOI: https://doi.org/10.30564/jmer.v4i2.3381

gauge. This energy corresponds to the difference in potential energy of the pendulum hammer before and after the impact. The results got from absorbed energy as a function of temperature and brittleness index for the specimens can be seen in Table 3.

Table 3. Values of energy absorbed in the impact test for the 3 samples.

Steel Samples	Sample 1 (Joules)	Sample 2 (Joules)	Sample 3 (Joules)	Average (Joules)
Melting zone - Longitudinal	158	54	146	119,3
Melting zone - Transverse	68	80	94	80,7
Heat-affected zone - Transverse	40	42	58	46,7

Source: Prepared by the authors, 2021.

First, the surfaces of the samples tested differed according to the fracture mode, comparing the longitudinal fracture specimens and the transversal weld fracture specimens (Figure 12). For steel specimens with fracture initiated by the melting zone, the fracture occurred irregularly, featuring a triaxiality of tensions, while those fractured in the heat-affected zone (ZAC), transversely to the weld showed a surface with greater flatness. The results verified in Table 3 also reveal a very strong divergence of values (more than 60%).

It is observed that in the heat-affected zone (ZAC) region, compared to the other regions, lower values of impact energy were recorded due to microstructural changes caused by the thermal cycle in welding. This thermal cycle leads to a heat-affected zone (ZAC), with the possible presence of martensite in the microstructure, resulting in lower fracture toughness. This fact, together with the discontinuity and porosities in the welding, corroborates the fact that the impact energy is lower in the transverse heat-affected zone (ZAC).

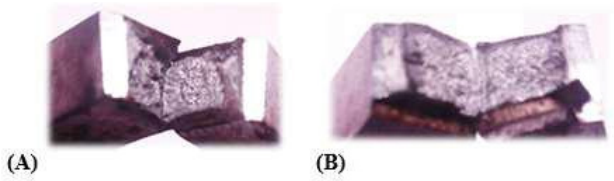

Figure 12. Comparative fracture images between a Charpy impact steel specimens. for longitudinal steel melt zone with pronounced irregularity on the fractured surface (A) and transverse heat-affected zone (ZAC), with a surface with greater flatness.

Source: Prepared by the authors, 2021.

5.4 Tensile Test

In the tensile test made for the base metal according to ASTM A370-10 [10] standard, although the extracted specimens are aligned in the rolling direction, the results of the values of the yield limit, rupture limit, maximum stress, and elongation, can be seen in Table 4.

The test specimens for the weld joints were not successful in the test, given the rupture in the weld region. This behavior is due to the welding failures found in the beads, causing a decrease in area and stress concentration, as well as the possible formation of embrittlement micro-constituents such as martensite arising from the cooling process of the bead.

Table 4. Yield limit, rupture limit, maximum stress and elongation values in the tensile test for the base metal and welded joint.

BASE METAL				
Steel specimens	Yield limit (MPa)	Rupture limit (MPa)	Maximum stress (MPa)	Elongation (%)
1	265	310	376	35
2	225	325	391	28,5
3	235	310	370	35,5
WELDED JOINT				
1	275	265	----------	---------
2	265	331	----------	---------

Source: Prepared by the authors, 2021.

 DOI: https://doi.org/10.30564/jmer.v4i2.3381

5. Conclusions

The "tests made from the parameters chosen in the autogenous laser welding of SAE 1020 steel with a thickness of 3/8", using a 10 kW IPG fiber laser model YLS-10000 at a speed of 2.4 m/min and focus - 6 mm was a priori satisfactory in external aspect. The experimental adjustments, compared with the literature of tests carried out with the same steel, with the same thickness, and with the same equipment, tended to make the process repeatable. However, when analyzing the cross-sections of the samples, discontinuities, porosities, lack of welding, geometric variations in the weald profile along with the depth, and significant microstructural changes were also verified in the mechanical tests. These deleterious defects led to the failure of those welded specimens submitted to the tensile test that broke in the joint, disqualifying the process, seen in Table 4.

The increase in hardness in the heat-affected zone (ZAC) in over 75% in the intermediate part of the weld in relation to base metal indicates the possibility of martensitic formation in this region, even though it is low carbon steel. This possibility is even more emphasized when compared to the Charpy impact energy in this region with an average of 46.6 J in the transverse heat-affected zone (ZAC), seen in Table 3.

One aspect that can be associated with variations in hardness and toughness and consequently with microstructural modifications is the large geometric variation in the weld profile seen in Figure 8, showing a variation in cooling rates along with the profile, which allows for microstructural change.

The low speed associated with the low power can influence the verified porosity and discontinuity (not forming the keyhole in the entire thickness of the plate).

This indicates that for a safe welding process with repeatable results, there may be other conditions with sensitive implications for the last quality. This influence can be verified not only in the equipment process parameters but also in the dimensional characteristics of the parts themselves (joint linearity, thickness) and their fastenings (joint alignment), as well as the welded regions of the parts given the thermal flow with relation to mass and conductivity to the environment.

References

[1] MAIMAN, T.H. Simulated optical radiation in ruby. Nature, v. 187, p. 493-494, 1960.

[2] STEEN, W. M. Laser material processing, SpringerVerlag, ISBN 1852336986. 2005.

[3] MENDEZ, P. F.; EAGAR, T. W. Penetration and defect formation in high-current arc welding. Welding Journal, p. 296- 306, 2003.

[4] LEIDINGER, D., et al. Improved manufacturing processes with high power lasers. Infrared Phys. Technol. vol. 36, No. 1, Great Britain, 251-266 p ,1995.

[5] LADARIO, P. F et.al A study of the laser welding process of automotive blanks, with and without coating, in the industrial environment aiming at incremental improvements and cost reduction. Pág. 02, 2009.

[6] CARVALHO S. M. Study of laser and TIG weldability of commercially pure grade 2 titanium used in aircraft pneumatic systems. Thesis - USP, Lorena, Brazil,2012.

[7] SAUCEDO, F. V., et al. Industrial Laser solutions for manufacturing, 2016. [Online]. Disponível em: [Acesso em: 10- Out-2016].

[8] BELFORTE, D. Tailor blank welding in Europe. Industrial Laser Solutions, USA, v. March, 2002.

[9] HITZ, C. B., EWING, J. J., HECHT J. Introduction to Laser Technology. 4. ed. Piscataway: Wiley-IEEE Press, 2012. 312 p.

[10] ABNT-Brazilian Association of Technical Standards - NBR NM-87-2000 - Carbon Steel and Alloys for Mechanical Construction - Designation and chemical composition. Available in: https://vdocuments.com.br/nbr-nm-87-2000-aco-carbono-e-ligados-para-construcao-mecanica-designacao.html.

[11] BUEHLER SUM-MET - The Science Behind Materials Preparation. ISBN 0-9752898-0-2, 2004.

[12] ASTM A370-10. Standard Test Methods and Definitions for Mechanical Testing of Steel Products. Available in: https://www.astm.org/Standards/A370.htm.

[13] API Standard 1104, 21st Edition is the industry standard for welding practices. Available in: https://pdfcoffee.com/api-1104-05bilinguecorpo-da-norma-pdf-free.html.

[14] A370-20 Standard Test Methods and Definitions for Mechanical Testing of Steel Products yield - Tension test - Charpy impact test/ Izod. Available in: https://www.astm.org/DATABASE.CART/HISTORICAL/A370-17.htm.

[15] ASTM E92-82 - Standard Test Method for Vickers Hardness of Metallic Materials. Available in: https://www.astm.org/Standards/E92.htm.

DOI: https://doi.org/10.30564/jmer.v4i2.3381